A versatile class of prototype dynamical systems for complex bifurcation cascades of limit cycles

Bulcsú Sándor[1] **and Claudius Gros**[1,*]

[1]Institute for Theoretical Physics, Goethe University Frankfurt, Frankfurt am Main, 60438, Germany
[*]gros@itp.uni-frankfurt.de

ABSTRACT

We introduce a versatile class of prototype dynamical systems for the study of complex bifurcation cascades of limit cycles, including bifurcations breaking spontaneously a symmetry of the system, period doubling bifurcations and transitions to chaos induced by sequences of limit cycle bifurcations. The prototype system consist of a $2d$-dimensional dynamical system with friction forces $f(V(\mathbf{x}))$ functionally dependent exclusively on the mechanical potential $V(\mathbf{x})$, which is typically characterized, here, by a finite number of local minima.
We present examples for $d = 1,2$ and simple polynomial friction forces $f(V)$, where the zeros of $f(V)$ regulate the relative importance of energy uptake and dissipation respectively, serving as bifurcation parameters. Starting from simple Hopf- and homoclinic bifurcations, complex sequences of limit cycle bifurcation are observed when energy uptake gains progressively in importance.

Introduction

The notion of a prototypical dynamical system is used whenever a certain system allows to study a certain relevant phenomenon, being at the same time simple enough that it is amendable for numerical and (at least partial) analytic investigations, without showing additional properties which could obfuscate the study of the prime phenomenon of interest.[1–3] Additionally, their dynamical behavior can often be understood in terms of general concepts, such as energy balance, symmetry breaking, etc.

Examples of prototype systems are the normal forms of standard bifurcation analysis[4,5] and classical systems, like the Van der Pol oscillator[4] or the Lorenz model,[6] which have been of central importance for the development dynamical system theory. As an example we consider the Liénard equation

$$\ddot{x} + f(x)\dot{x} + g(x) \;=\; 0\;, \tag{1}$$

a generic adaptive mechanical system, which includes the Van der Pol oscillator and the Takens-Bogdanov system.[7,8] The periodically forced extended Liénard systems with a double-well potential have also been studied by many authors (see e.g. the double-well Duffing oscillator[9–11]).

In this paper we propose a new class of autonomous Liénard-type systems, which allows to study cascades of limit cycle bifurcations using a bifurcation parameter controlling directly the balance between energy dissipation and uptake, and hence the underlying physical driving mechanism. Though there are a range of construction methods for dynamical systems in the literature (see e.g.[12–14]), they tend however to assume a somewhat abstract view, such as starting from implicitly defined manifolds, or involve mathematical tools accessible only to researchers with an in-depth math training. In contrast to these methods, we provide here a mechanistic design procedure, based on the construction of attractors by the use of potentials, a concept often used in many interdisciplinary fields (e.g. in modeling cardiovascular systems[15] or for solving optimization problems[16]), making it easily accessible and implementable for other scientific communities (such as neuroscience, biology etc.) as well.

As an introductory example for the role of balance between energy uptake and dissipation in both local and global bifurcations we reconsider the Bogdanov-Takens system,

$$\ddot{x} = (x-\mu)\dot{x} - V'(x), \qquad \begin{aligned} \dot{x} &= y \\ \dot{y} &= (x-\mu)y - V'(x)\;, \end{aligned} \tag{2}$$

which is often used as a prototype system for homoclinic bifurcations.[4] Here, the mechanical potential is a third order polynomial, as illustrated in Fig. 1. The friction force is directly proportional to the velocity y and fixpoints of (2) correspond hence to the minima and the maxima of the potential $V(x)$.

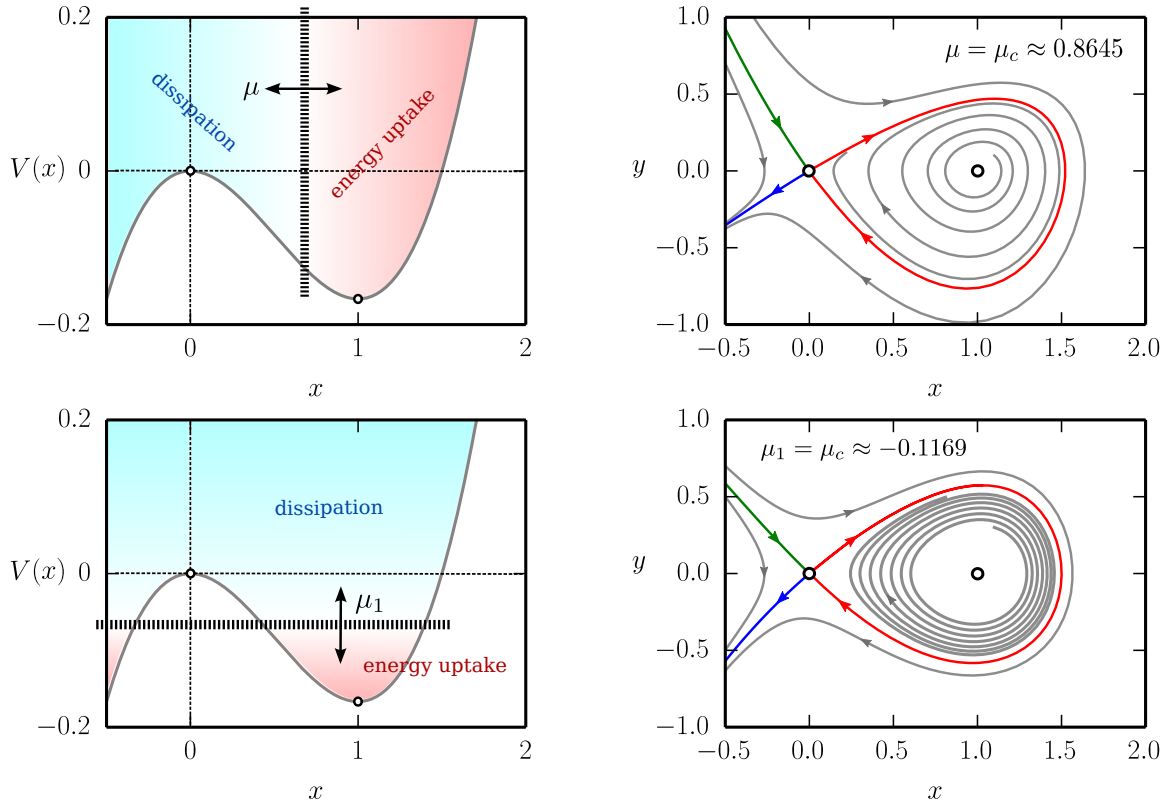

Figure 1. The Bogdanov-Takens system (2) with the potential function $V(x) = x^3/3 - x^2/2$ and a friction term $x - \mu$ (*top row*), and its generalization (4) to a friction term $\mu_1 - V(x)$ (*bottom row*), compare Eq. (6). *Left column*: The potential function together with the color-coded regions of respectively energy dissipation and uptake, compare Eq. (3). *Right column*: The phase planes at the respective homoclinic bifurcation points, with the respective unstable foci and the saddles by open circles. The green and blue trajectories are the stable and unstable manifolds and the red trajectory corresponds to the homoclinic loop.

The dynamics of the Bogdanov-Takens system is controlled by the parameter μ, defining, in terms of the mechanical energy E, the regions of dissipation and energy uptake in the potential valley,

$$\dot{E} = (x-\mu)y^2, \qquad E = \frac{y^2}{2} + V(x)\ , \tag{3}$$

compare Fig. 1. The region $x > \mu$ of energy uptake increases when the bifurcation parameter μ is decreased, leading to two consecutive transitions. Initially the potential minimum becomes repelling, undergoing a supercritical Hopf bifurcation and a stable limit cycle emerges. Decreasing μ further the extension of the limit cycle increases, merging at μ_c with the stable and unstable manifolds of the saddle, resulting in a homoclinic bifurcation.

Results

The key mechanism leading to a bifurcation in the Bogdanov-Takens systems is the availability of a parameter allowing to change the balance between energy uptake and energy dissipation along limit cycles. Our aim is to generalize this idea to the case of mechanical systems characterized by an arbitrary number of potential minima. For this purpose we consider with

$$\begin{aligned} \dot{\mathbf{x}} &= \mathbf{y} \\ \dot{\mathbf{y}} &= f(V(\mathbf{x}))\mathbf{y} - \nabla V(\mathbf{x}) \end{aligned} \qquad \dot{E} = f(V(\mathbf{x}))\mathbf{y}^2 \tag{4}$$

a $2d-$dimensional system, with d spatial coordinates and with friction forces depending via $f(V(\mathbf{x}))$ functionally only on the mechanical potential $V(\mathbf{x})$, allowing a fine-tuned control of the energy dissipation and uptake around the respective potential

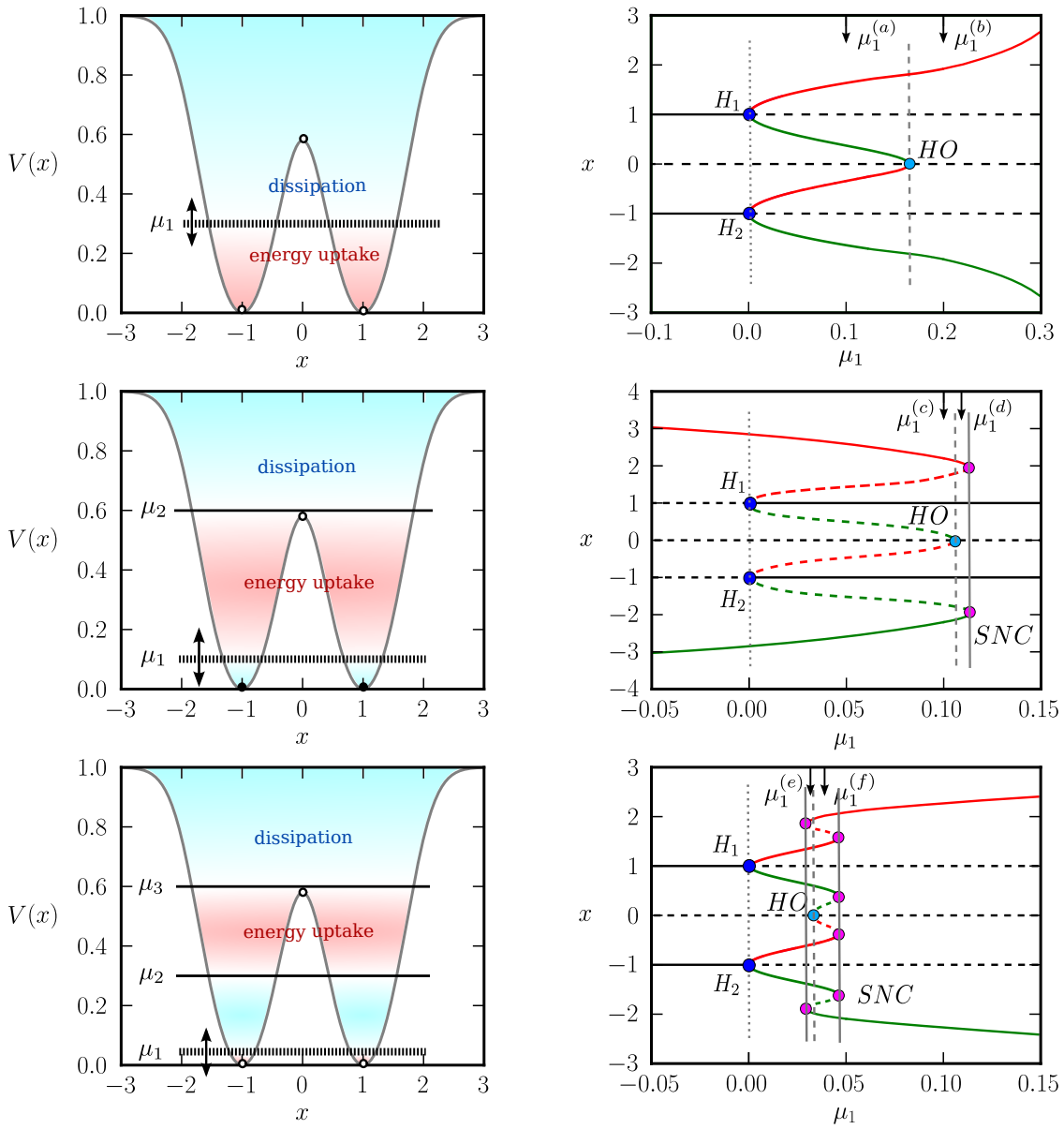

Figure 2. *Left column*: Double well potential, as defined by Eq. (7) and with $x_{1,2} = \pm 1$, $V_{1,2} = 0$, $z_{1,2} = 1$ and $p_{1,2} = 1$. The regions of energy dissipation $\dot{E} < 0$ and uptake $\dot{E} > 0$ are color coded. For the friction functions (6) we used f_1, with $\alpha = 1$ (*top row*), f_2, with $\mu_2 = 0.6$ and $\alpha = 5$ (*middle row*), and f_3, with $\mu_2 = 0.3$, $\mu_3 = 0.6$ and $\alpha = 5$ (*bottom row*). *Right column*: Bifurcation diagrams of the respective generalized Liénard systems (4), as a function of μ_1. All other μ_i (when present) are kept constant. Stable/unstable fixpoints or limit cycles are denoted by continuous/dashed curves respectively. Black lines are fixpoint lines, while the maximal/minimal amplitude of x in a cycle is denoted with red/green color. H points denote Hopf-bifurcations, *HO* corresponds to homoclinic bifurcations of a saddle, *SNC* points denote saddle node bifurcations of limit cycles. The dotted, dashed and continuous vertical gray lines are just guides for the eyes.

minima. A well known example of the system of type (4) is the Van der Pol oscillator

$$\ddot{x} - \varepsilon\left(1 - x^2\right)\dot{x} + x = 0, \qquad f(V) = \varepsilon(1 - 2V), \qquad V(x) = \frac{x^2}{2}, \tag{5}$$

for which the regions of energy uptake and dissipation remain fixed, with ε regulating the overall influence of the velocity-dependent force.

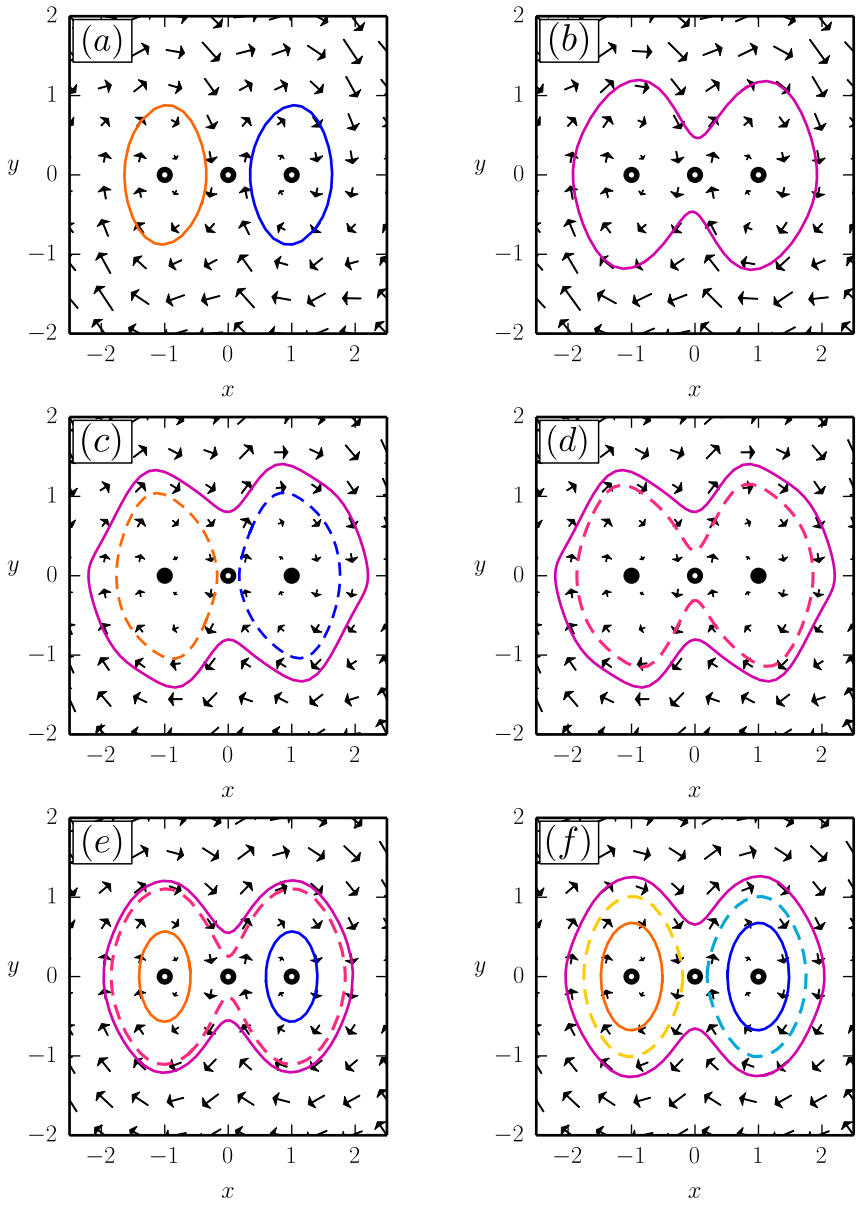

Figure 3. Flow diagrams for the systems presented in Fig. 2, using respectively linear / quadratic / cubic friction functions $f_1(V)$ / $f_2(V)$ / $f_3(V)$ (*top/middle/bottom row*). The values $\mu_1^{(a/b)} = 0.1/0.2$, $\mu_1^{(c/d)} = 0.1/0.11$ and $\mu_1^{(e/f)} = 0.032/0.04$ for the respective μ_1 are indicated by arrows in the corresponding bifurcation diagrams in Fig. 2.

The simplest generic class of friction functions $f(V)$ entering (4) are polynomial:

$$f_1(V) = -\alpha(V-\mu_1), \qquad f_2(V) = -\alpha(V-\mu_1)(V-\mu_2), \qquad f_3(V) = -\alpha(V-\mu_1)(V-\mu_2)(V-\mu_3), \tag{6}$$

where α regulates the overall strength of the friction and where the individual $\mu_1 < \mu_2 < \mu_3$ are the respective zeros, the points at which dissipation changes to anti-dissipation and vice-versa, compare Fig. 2.

When using $f_1(V)$ and the mechanical potential $V(x) = x^3/3 - x^2/2$, the resulting flow in phase space is equivalent to the one of the Bogdanov-Takens system (2), as shown in Fig. 1.

Generalized mechanical potentials

We are interested in using (4) as prototype dynamical systems, especially for the case of non-trivial mechanical potentials $V(\mathbf{x})$ having an arbitrary number M of local minima. One could in principle consider higher-order polynomials for this purpose,

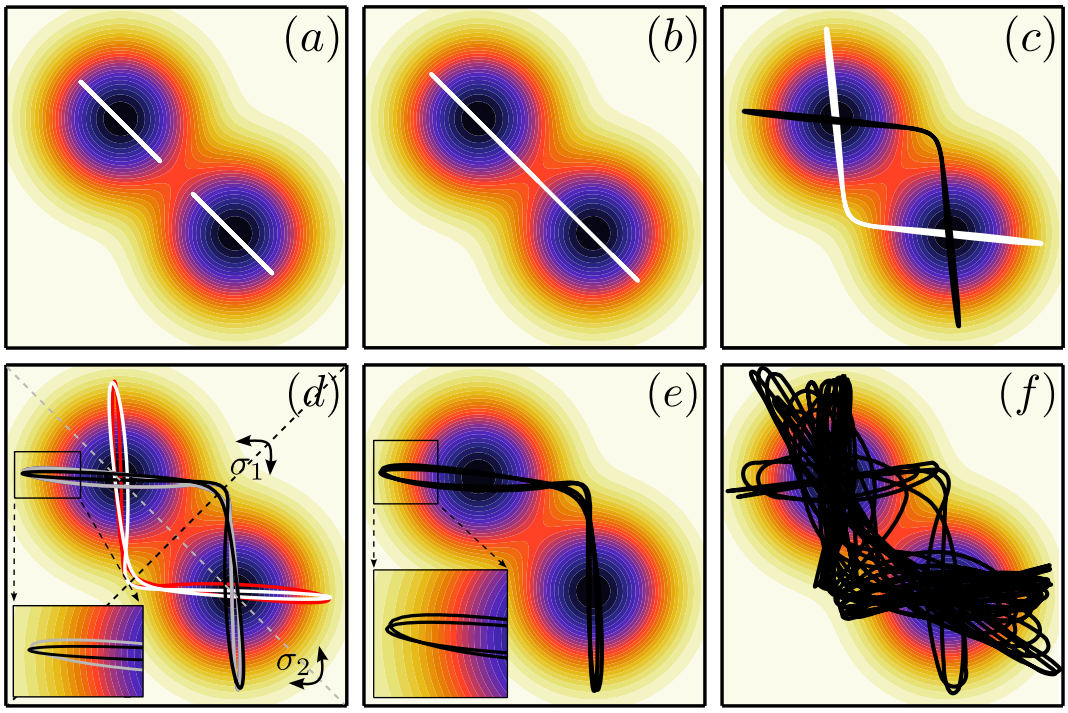

Figure 4. Stable limit cycles and chaotic orbits of the Liénard prototype system (4) in a two-dimensional symmetric double well potential $V(\mathbf{x})$ (color coded, as defined by Eq. (9)) and with a linear friction term $f_1(V(\mathbf{x})) = 0.5(\mu_1 - V(\mathbf{x}))$. The bifurcation parameter μ_1 is $0.1, 0.15, 0.25, 0.265, 0.2698, 0.3$ from (a) to (f). In (d) the four limit cycles can be mapped into each other by using the symmetry operations $\sigma_{1,2}$ or $\sigma_{3,4}$, as discussed in the Methods section. For (e) only a single of the four stable limit cycles is shown. This needs to circle the two potential minima twice in order to retrace itself. In (f) an example of a chaotic trajectory is given.

however they do not allow to control the overall height of the potential and the relative width of the local minimal in as simple fashion.

For this purpose we use throughout this study potential functions of the kind

$$V(\mathbf{x}) = \prod_n \left(g_n(\mathbf{x} - \mathbf{x}_n) + \frac{V_n}{p_n} \right), \qquad g_n(\mathbf{z}) = \tanh(\mathbf{z}^2 / {z_n}^2) \,, \tag{7}$$

where the $z_n > 0$ determine the half-width of the respective local minima and where the p_n satisfy the self-consistent condition:

$$p_n = \prod_{m \neq n} \left(g_n(\mathbf{x}_n - \mathbf{x}_m) + \frac{V_m}{p_m} \right), \qquad V(\mathbf{x}_n) = \frac{V_n}{p_n} \prod_{m \neq n} \left(g_n(\mathbf{x}_n - \mathbf{x}_m) + \frac{V_m}{p_m} \right) = V_n \,, \tag{8}$$

since $g(0) = 0$. For deep minima, with $(z_i + z_j) \ll |\mathbf{x}_i - \mathbf{x}_j|$, the positions and the heights of the local minima are close to $\mathbf{x}_n$ and V_n respectively. We found, that a relative accuracy of 10^{-2} for V_n can already be achieved in general after three or four iterations.

Limit cycle bifurcation cascades

The system of type (4) allows to describe complex cascades of limit cycle bifurcations and in Fig. 2 we show some illustrative examples using a symmetric double-well potential and linear / quadratic / cubic friction functions $f_1(V)$ / $f_2(V)$ / $f_3(V)$ respectively, see Eq. (6). We used numerical methods[17] to obtain the respective full bifurcation diagrams, with solid/dashed lines denoting stable/unstable fixpoints and limit cycles. The corresponding flow in phase space is illustrated in Fig. 3.

For negative μ_1 values the two fixpoints $(\pm 1, 0)$ are stable, for the case of $f_1(V)$ and $f_3(V)$, and stable limit cycles evolve via two supercritical Hopf-bifurcation. For $f_2(V)$, on the other side, a sub-critical Hopf bifurcation is observed at $\mu_1 = 0$. The respective stable/unstable limit cycles merge for $f_1(V)$ and $f_2(V)$ in a homoclinic bifurcation, whereas a more complex bifurcation diagram emerges for $f_3(V)$. Saddle node bifurcation of limit cycles are present for both $f_2(V)$ and $f_3(V)$.

Chaos via period doubling of limit cycles

We consider now a prototype system (4) with a two-dimensional symmetric potential field $V(\mathbf{x})$,

$$V(\mathbf{x}) = g(\mathbf{x}-\mathbf{x}_1)g(\mathbf{x}-\mathbf{x}_2), \qquad g(\mathbf{z}) = \tanh(4\mathbf{z}^2/9)\ , \tag{9}$$

as defined in (7), having two minima $\mathbf{x}_{1,2} = \pm(1,-1)$, and a linear friction term $f_1(V) = 0.5(\mu - V)$. Both diagonals in the (x_1,x_2) are symmetries of the system, as discussed in the Methods section. In Fig. 4 we present examples of stable limit cycles and of a chaotic trajectory, as projected to the (x_1,x_2) plane. In Fig. 5 the corresponding bifurcation diagram is presented, which shows Hopf bifurcations (H), homoclinic bifurcations (HO), branching of limit cycles via spontaneous symmetry breaking (SSB), period doubling of limit cycles (PD) and a transition to chaotic behavior:

H At $\mu_1^{(H)} = 0$ the two potential minima become unstable, just as for the one-dimensional spatial system presented in Fig. 2, resulting in two equivalent super-critical Hopf bifurcations. We note that, as a result of the symmetric potential function (9), a second branch of limit cycles is created by the two Hopf bifurcations (see the discussion in the Methods section and the Supplementary Information). However, since in the parameter region of interest these limit cycles are mostly unstable, we have not investigated them in detail.

HO At $\mu_1^{(HO)} \approx 0.143$ the limit cycles merge, as in Fig. 4(a) $\rightarrow$ (b), in a homoclinic transition. The limit cycle stays, however, exactly on the diagonal $x_1 + x_2 = 0$.

SSB At the first branching point of limit cycles, $\mu_1^{(SSB)} \approx 0.171$ the symmetry with respect to the diagonal $(1,-1)$ is spontaneously broken, as in Fig. 4(b) $\rightarrow$ (c), with the two limit cycles still being symmetric with respect to the $(1,1)$ diagonal. The latter symmetry is broken at the second branching point $\mu_1^{(SSB)} \approx 0.260$, as in Fig. 4(c) $\rightarrow$ (d), with four symmetry related limit cycles being stable.

PD For larger values of the bifurcation parameter μ_1 a series of period-doubling of limit cycles is observed, with the first occurring at $\mu_1^{(PD)} \approx 0.268$, as in Fig. 4(d) $\rightarrow$ (e). The next period-doubling transition occurs at $\mu_1^{(PD)} \approx 0.270$, as shown in Fig. 5.

For reference we note, that the saddle of the potential is located at $V(0,0) = 0.505$, viz at a substantially larger value.

For $\mu_1 > \mu_1^{(chaos)} \approx 0.2705$ we observe seemingly chaotic trajectories, as illustrated in Fig. 4(f). Studying the transition to chaos is not the subject of the present investigation and we leave it to future work. We presume however, that the transition occurs via an accumulation of an infinite number of of period-doubling transitions of limit cycles, similar to the ones observed for the Lorenz system[18] and for the Rössler attractor.[19,20]

Our prototype system (4) is not generically dissipative. We have evaluated the average contraction rate σ, as defined by (22) in the Methods section, and present the results in Fig. 5. Phase space contracts trivially along the attracting limit cycles, but also, on the average, in the chaotic region, where the average Lyapunov exponent λ becomes positive. λ is negative also for $\mu_1 < 0$, when only stable fixpoints are present, vanishing for intermediate values of μ_1, when stable limit cycles are present. The later is due to the fact, see Fig. 7 and the corresponding Methods section, that two initially close trajectories will generically flow to the same limit cycle with the relative distance becoming then constant.

For larger values of $\mu_1 > 0.322$ the chaotic region transients into a phase of intermittent chaos as illustrated in Fig. 6, in which an extended quasi-regular flow along the $(-1,1)$ diagonal is interseeded by a roughly perpendicular bursting flow. This behavior is, to a certain extend, reminiscent to a scenario of intermittent chaos,[21] in which a strange attractor is embedded in a higher-dimensional space with partly unstable directions. We have, however, not investigated the observed intermittent dynamics in detail.

Discussion

We have proposed and discussed a prototype dynamical system (4) in which the friction forces $\propto f(V)$ depend functionally only on the mechanical potential $V(\mathbf{x})$. We have shown, that complex cascade of limit cycle bifurcation can be obtained even for two dimensional phase spaces when the friction function $f(V)$ alternates between regions of energy uptake and dissipation.

We have also introduced a generic class of potential functions (7) which allow to define, in a relative straightforward manner, mechanical potentials with an arbitrary number of local minima with varying depth. Any other potential could be however used. For example one could study the biquadratic version

$$V(\mathbf{x}) \ \rightarrow\ \left(\mathbf{x}-\mathbf{x}_1\right)^2\left(\mathbf{x}-\mathbf{x}_2\right)^2 \tag{10}$$

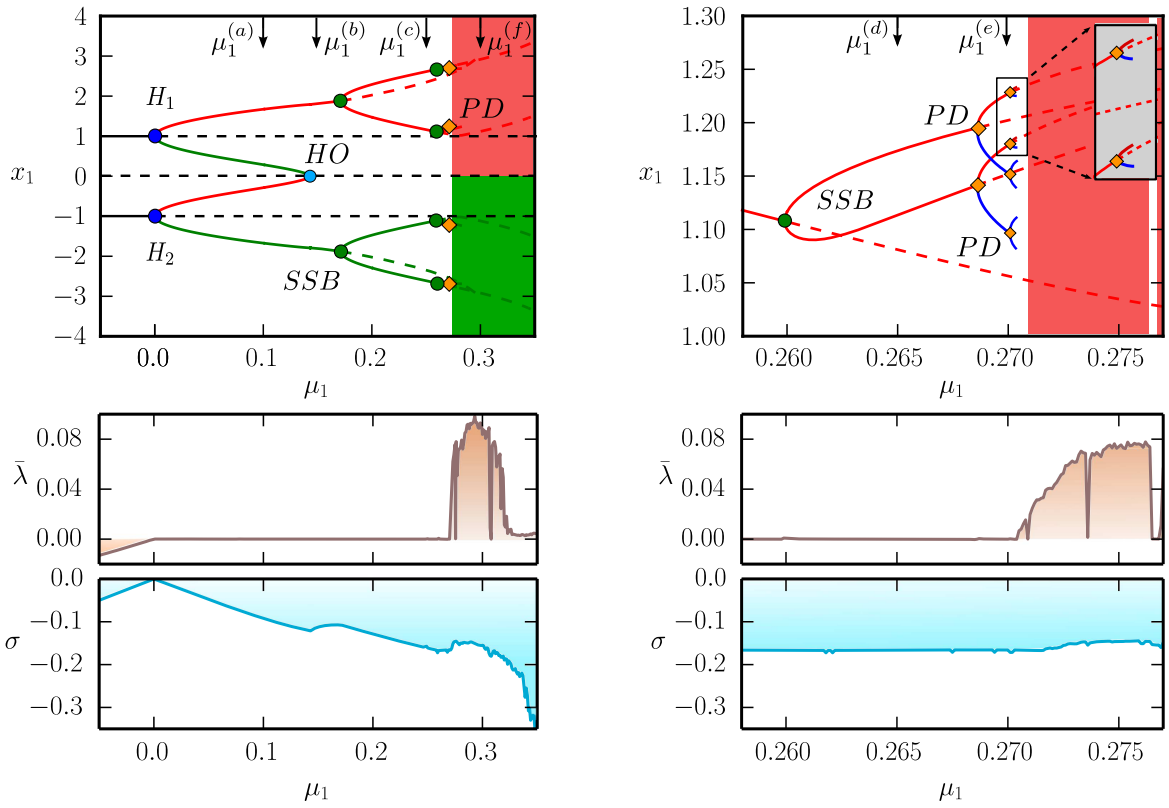

Figure 5. *Top row*: The numerically obtained bifurcation diagram for a two dimensional prototype Liénard system with symmetric double-well potential and a linear friction force, as for Fig. 4. The second branches of limit cycles emerging from the two destabilized minima (see Supplementary Fig. S1) are not shown here. One observes Hopf and homoclinic bifurcations (H and HO), branching of limit cycles via spontaneous symmetry breaking and period doubling (SSB and PD), as well a transition to chaos for $\mu > 0.2705$. The red/green lines indicate the maximal/minimal x_1-values of the respective limit cycles. The blue curve is the second x_1-maxima after period doubling. The right diagram represents a zoom-in of the transition to a chaotic region, indicated by the shaded green and red areas. Only the first two period doubling bifurcations are shown. *Bottom row*: The average Lyapunov exponent $\bar{\lambda}$ and the contraction rate σ, calculated as described in the Methods section, for the corresponding μ_1 parameter intervals. For the left figure $\Delta\mu_1 = 0.001$ parameter stepsize was used. Increasing the resolution more and more periodic windows (with $\bar{\lambda} = 0$) become visible, as shown on the right plot, where $\Delta\mu_1$ is decreased with a factor of ten.

of the potential (9) used in our study of chaotic behavior with the prototype system (4). We did not study in detail the bifurcation diagram for the potential function (10), presume however, that it would be similar to the results presented in Fig. 4 and 5, having the same underlying driving mechanism in terms of a linear friction function $f(V) \propto (\mu_1 - V)$.

We have shown that a simple double-well prototype system with two spatial dimensions (and with a four-dimensional phase space) shows both symmetry induced bifurcations of limit cycles together with a period-doubling of limit cycle transition to chaotic behavior.

As a future perspective we note, that by changing the depth of the minima, one could control the order in which the fixpoints are going be destabilized, which might lead to other interesting phenomena. Adding an extra (maybe slow) dynamics to the positions or heights of the minima, the metadynamics of the attractors[22] may also be considered. In this case the p_n parameters should be recalculated in each time-step using the self-consistent equations (8), which proved to be fast enough for practical purposes.

Models, for which the equations of motion are derived from higher order principles, provide promising results for the understanding many different phenomena, such as the optimization hardness of boolean satisfiability problems[16] or the complex dynamics of biological neural networks.[23,24] Generally, these methods involve the construction of a generating functional, such as the cost function or energy functional,[25–28] with the dynamics of the system being defined by a gradient decent rule. When all equations are derived from the same generating functional, the system corresponds mathematically to a gradient system for which the asymptotic behavior is determined by the stable fixpoints (nodes). Thus they can not produce limit

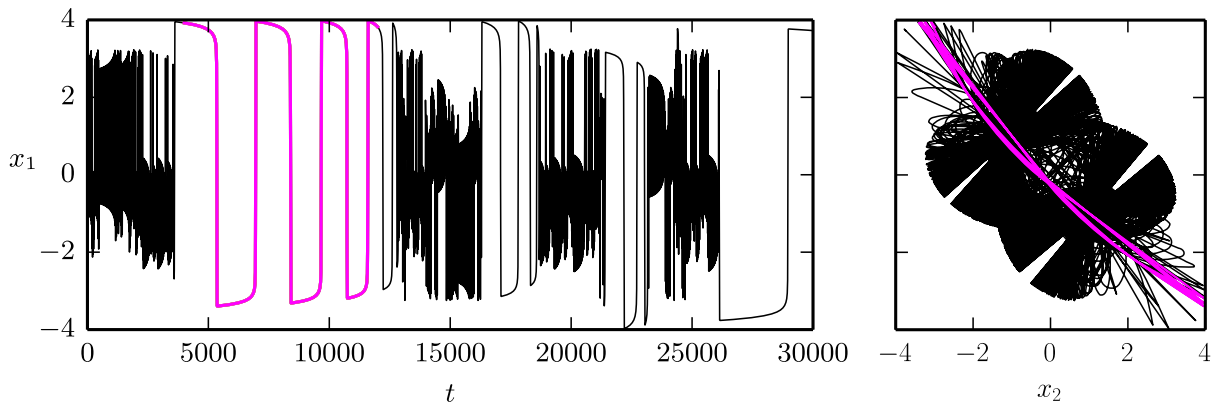

Figure 6. *Left*: Quasi-periodic windows with different time scales in the time-series plot of x_1 variable for $\mu_1 = 0.34$. *Right*: Phase space plot of the trajectory projected to the (x_1, x_2) plane for the same parameter. The magenta curve corresponds to the $t_p = [4 \cdot 10^3, 12 \cdot 10^3]$ quasi-periodic time interval, denoted with the same color in the $x_1(t)$ plot.

cycles or any oscillatory behavior. To by-pass this problem, usually additional equations of motions are defined, derived either from a second generating functional to produce objective function stress[29,30] or from other considerations. In our model, the system has an inherent inertia, which leads to damped oscillations around equilibria (minima of the potential) in the presence of dissipation. By creating regions of antidissipation, stable oscillatory dynamics and chaotic behavior can also be achieved. Considering nonsymmetric, higher dimensional potential functions we expect to find an even richer set of dynamical behaviors (see the Methods section), a scenario worth be investigated in the future.

Finally, we note that the concepts of dynamical systems theory, such as attractors, slow points and bifurcations have been used recently to understand phenomena of surprisingly diverse fields. For examples of some relevant applications we mention here the modeling of birdsong,[31] migraine[32] dynamics and the control mechanisms developed for the movements of humanoid robots.[33] Hence, we believe that prototype systems which allow the construction of models with predefined attractors in an intuitive manner could offer a useful tool for understanding the behavior of interesting interdisciplinary problems.

Methods

Hopf bifurcations in the prototype system

2-dimensional prototype systems

The local maxima of the potential function, i.e. where $V''(x^*) < 0$, which are saddle points, separate the phase plane into different attraction domains with their stable manifold. Local minima with $V''(x^*) > 0$ become, on the other hand, repelling focuses as a result of an Andronov-Hopf bifurcation, when dissipation changes to antidissipation in their neighborhood, having a simple pair of purely imaginary eigenvalues $\lambda_{1,2} = \pm i\sqrt{V''(x^*)}$.

4-dimensional prototype systems

Analogously, the

$$\mathbf{q}^* = (x_1^*, x_2^*, y_1^*, y_2^*), \qquad y_{1,2}^* = 0, \qquad \left.\frac{\partial V(x_1,x_2)}{\partial x_{1,2}}\right|_{x_1^*,x_2^*} = 0$$

fixpoints of the 4-dimensional prototype systems (4) correspond to critical points of the $V(x_1, x_2)$ potential function. Classification of the local minima and saddle critical points with respect to their stability can be achieved by evaluating the eigenvalues of the Jacobian of the system in terms of the Hessian of the potential function:

$$J(\mathbf{q}^*) = \begin{pmatrix} 0 & 0 & 1 & 0 \\ 0 & 0 & 0 & 1 \\ d_1 & c & a & 0 \\ c & d_2 & 0 & a \end{pmatrix}, \qquad H(x_1^*, x_2^*) = \begin{pmatrix} -d_1 & -c \\ -c & -d_2 \end{pmatrix} \tag{11}$$

where we have defined with

$$a = f(V(x_1^*, x_2^*)), \qquad c = -\left.\frac{\partial^2 V}{\partial x_1 \partial x_2}\right|_{x_1^*,x_2^*}, \qquad d_{1,2} = -\left.\frac{\partial^2 V}{\partial x_{1,2}^2}\right|_{x_1^*,x_2^*} \tag{12}$$

the friction term and the second order partial derivatives of the potential at the respective critical points. Defining with

$$\gamma_{\pm} = \frac{1}{2}\left(-(d_1+d_2) \pm \sqrt{(d_1+d_2)^2 - 4(d_1 d_2 - c^2)}\right), \qquad \gamma_{\pm} \in \mathbb{R} \tag{13}$$

we can express the eigenvalues of the Jacobian $J(\mathbf{q}^*)$ as

$$\lambda_{1,2,3,4} = \frac{1}{2}\left(a \pm \sqrt{a^2 - 4\gamma_{\pm}}\right). \tag{14}$$

For general potential functions the local minima, defined by the $\Delta = \det(H) = d_1 d_2 - c^2 > 0$ and $\rho = \mathrm{tr}(H) = -(d_1 + d2) < 0$ conditions (or equivalently by $\gamma_{\pm} > 0$), undergo a Hopf bifurcation, when the $f(V)$ friction term changes sign, i.e.:

$$a = f(V(x_1^*, x_2^*)) = 0 \qquad \Rightarrow \qquad \lambda_{1,2,3,4} = \pm i\sqrt{\gamma_{\pm}}. \tag{15}$$

However, saddles of the potential function, i.e. $\Delta = \det(H) < 0$, are saddle type fixpoints of the dynamical system, having always a λ_1 positive eigenvalue, as $\gamma_+ > 0$ and $\gamma_- < 0$.

Here we note that in case of the potential function (9), due to the symmetries one gets a double pair of imaginary eigenvalues, since $d_1 = d_2$ and $c = 0$, and thus Eq. (13) yields $\gamma_+ = \gamma_-$. This results in a second branch of limit cycle solutions, not investigated in this paper, emerging from the Hopf-point.

2d-dimensional prototype systems

For arbitrary dimensions d one can express the Jacobian in terms of block matrices:

$$J(\mathbf{q}^*) = \begin{pmatrix} O_d & I_d \\ -H_d & aI_d \end{pmatrix}, \tag{16}$$

where $a = f(V)$ and where O_d and I_d are the d-dimensional zero and identity matrices. $H_d = (H_{i,j}(\mathbf{x}^*)) = \left(\frac{\partial^2 V}{\partial x_i \partial x_j}\Big|_{\mathbf{x}^*}\right)$ is the Hessian matrix of the $V(\mathbf{q})$ potential, evaluated for the respective $\mathbf{q}^* = (\mathbf{x}^*, \mathbf{y}^*)$ fixpoint.

To determine the eigenvalues of the Jacobian one has to solve the equation:

$$\det(J - \lambda I_d) = \begin{vmatrix} -\lambda I_d & I_d \\ -H_d & (a-\lambda)I_d \end{vmatrix} = \det(-\lambda(a-\lambda)I_d + H_d) = 0, \tag{17}$$

where we used the properties of square block matrices. By introducing $\gamma = \lambda(a-\lambda)$ on finds with

$$\det(J - \lambda I_d) = \det(H_d - \gamma I_d) = \prod_{i=1}^{d}(\gamma - \gamma_i) = 0 \tag{18}$$

that the $2d$ eigenvalues λ of the Jacobian can be expressed in terms of the d eigenvalues γ_i of the Hessian matrix and hence

$$\lambda_i^{\pm} = \frac{1}{2}\left(a \pm \sqrt{a^2 - 4\gamma_i}\right). \tag{19}$$

Consequently, at the local minima of the potential, i.e. when $\gamma_i > 0$, a Hopf-bifurcation occurs, with $\lambda_i^{\pm} = \pm i\sqrt{\gamma_i}$, when the friction term $a = f(V)$ changes sign. For general potential functions this might lead to the birth of higher dimensional tori or several branches of limit cycle bifurcations.

Symmetries of the 4-dimensional system

The results shown in Figs. 4, 5 and 6 are for a 4-dimensional prototype systems (4) with a linear friction force $f_1(V)$, as defined in (6), and a mechanical potential $V(\mathbf{x})$ given by (9). The minima $V(\mathbf{x}_{1,2}) = 0$ of the potential, viz. $\mathbf{x_1} = (+1,-1)$ and $\mathbf{x_2} = (-1,+1)$ are connected by the symmetry operations

$$\sigma_{1,2} = \begin{pmatrix} 0 & \pm 1 & 0 & 0 \\ \pm 1 & 0 & 0 & 0 \\ 0 & 0 & 1 & 0 \\ 0 & 0 & 0 & 1 \end{pmatrix}, \qquad \sigma_{3,4} = \begin{pmatrix} 0 & \pm 1 & 0 & 0 \\ \pm 1 & 0 & 0 & 0 \\ 0 & 0 & 0 & \pm 1 \\ 0 & 0 & \pm 1 & 0 \end{pmatrix} \tag{20}$$

of the system. Thus, if (x_1, x_2, y_1, y_2) is a solutions, then

$$\begin{pmatrix} x_1' \\ x_2' \\ y_1' \\ y_2' \end{pmatrix} = \sigma_{1,2}\begin{pmatrix} x_1 \\ x_2 \\ y_1 \\ y_2 \end{pmatrix}, \qquad \begin{pmatrix} x_1'' \\ x_2'' \\ y_1'' \\ y_2'' \end{pmatrix} = \sigma_{3,4}\begin{pmatrix} x_1 \\ x_2 \\ y_1 \\ y_2 \end{pmatrix} \tag{21}$$

are also solutions.

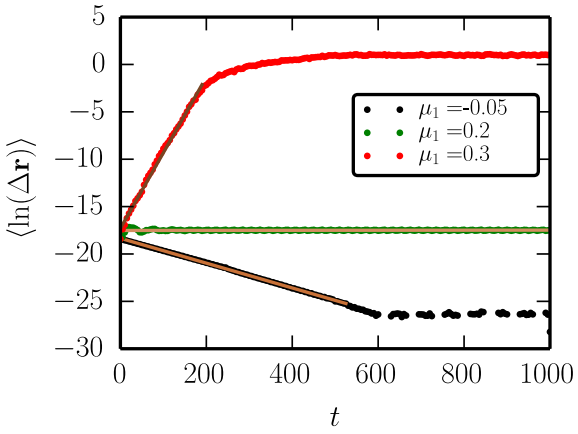

Figure 7. The logarithmic growth rate $\langle \ln(\Delta \mathbf{r}) \rangle$ averaged for 100 random initial conditions as a function of time for three qualitatively different types of dynamics: spiraling into a fixpoint ($\mu_1 = -0.05$), limit cycle oscillations ($\mu_1 = 0.2$) and chaotic behavior ($\mu_1 = 0.3$). Brown lines correspond to the best linear regression. In the first and last case, the line is fitted only to the first part of the trajectory. The dashed line indicates that the distance of the point pairs has reached the maximal accuracy of the integrator.

Lyapunov exponent and contraction rate

The local Lyapunov exponent λ is determined from the growth rate of the distance $\Delta \mathbf{r}(t) = \Delta \mathbf{r}_0 e^{\lambda t}$, between point pairs with an initial displacement, which we have taken to be $\Delta \mathbf{r}_0 = 10^{-8}$. Measuring the Lyapunov exponent was started after a transient of $t_{tr} = 1.5 \cdot 10^4$. Considering 100 random initial conditions the average Lyapunov exponent $\bar{\lambda}$ is then given by the slope of the initial linear part of the $\langle \ln(\Delta \mathbf{r}) \rangle$ curve (as given by the brown lines in Fig. 7).

The contraction rate σ, is defined as the average of local contraction rates along a set of trajectories Γ for different initial conditions:

$$\sigma = \left\langle \frac{1}{L} \int_\Gamma \nabla \cdot \mathbf{f} \, ds \right\rangle, \tag{22}$$

where $L = \int_\Gamma ds$ is the length of the trajectory and $\mathbf{f}$ is the flow, viz the right-hand side of the evolution equations (4). σ is negative for dissipative systems, in which the phase space contracts.[4,5]

References

1. Cymbalyuk, G. S., Calabrese, R. L. & Shilnikov, A. L. How a neuron model can demonstrate co-existence of tonic spiking and bursting. *Neurocomputing* **65**, 869–875 (2005).
2. Uçar, A. On the chaotic behaviour of a prototype delayed dynamical system. *Chaos, Solitons & Fractals* **16**, 187–194 (2003).
3. Krupa, M., Popovic, N. & Kopell, N. Mixed-mode oscillations in three time-scale systems: a prototypical example. *SIAM Journal on Applied Dynamical Systems* **7**, 361–420 (2008).
4. Gros, C. *Complex and adaptive dynamical systems: A primer* (Springer, 2013).
5. Chow, S.-N., Li, C. & Wang, D. *Normal forms and bifurcation of planar vector fields* (Cambridge University Press, 1994).
6. Lorenz, E. N. Deterministic nonperiodic flow. *Journal of the atmospheric sciences* **20**, 130–141 (1963).
7. Takens, F. Singularities of vector fields. *Publications Mathématiques de l'IHÉS* **43**, 47–100 (1974).
8. Bogdanov, R. I. Versal deformations of a singular point of a vector field on the plane in the case of zero eigenvalues. *Functional analysis and its applications* **9**, 144–145 (1975).
9. Venkatesan, A. & Lakshmanan, M. Bifurcation and chaos in the double-well duffing–van der pol oscillator: Numerical and analytical studies. *Physical Review E* **56**, 6321–6330 (1997).
10. Yamaguchi, A., Fujisaka, H. & Inoue, M. Static and dynamic scaling laws near the symmetry-breaking chaos transition in the double-well potential system. *Physics Letters A* **135**, 320–326 (1989).

11. Li, R., Xu, W. & Li, S. Chaos controlling of extended nonlinear liénard system based on the melnikov theory. *Applied Mathematics and Computation* **178**, 405–414 (2006).

12. Sandstede, B. Constructing dynamical systems having homoclinic bifurcation points of codimension two. *Journal of Dynamics and Differential Equations* **9**, 269–288 (1997).

13. Deng, B. Constructing homoclinic orbits and chaotic attractors. *International Journal of Bifurcation and Chaos* **04**, 823–841 (1994).

14. Qi, G., Du, S., Chen, G., Chen, Z. & Yuan, Z. On a four-dimensional chaotic system. *Chaos, Solitons & Fractals* **23**, 1671–1682 (2005).

15. Regan, E. R. & Aird, W. C. Dynamical systems approach to endothelial heterogeneity. *Circulation research* **111**, 110–30 (2012).

16. Ercsey-Ravasz, M. & Toroczkai, Z. Optimization hardness as transient chaos in an analog approach to constraint satisfaction. *Nature Physics* **7**, 966–970 (2011).

17. Clewley, R. Hybrid models and biological model reduction with pydstool. *PLoS Computational Biology* **8**, e1002628 (2012).

18. Robbins, K. Periodic solutions and bifurcation structure at high r in the lorenz model. *SIAM Journal on Applied Mathematics* **36**, 457–472 (1979).

19. Rössler, O. E. An equation for continuous chaos. *Physics Letters A* **57**, 397–398 (1976).

20. Gardini, L. Hopf bifurcations and period-doubling transitions in rössler model. *Il Nuovo Cimento B Series 11* **89**, 139–160 (1985).

21. Lai, Y.-C. Symmetry-breaking bifurcation with on-off intermittency in chaotic dynamical systems. *Physical Review E* **53**, R4267 (1996).

22. Gros, C., Linkerhand, M. & Walther, V. Attractor metadynamics in adapting neural networks. In *Artificial Neural Networks and Machine Learning – ICANN 2014*, vol. 8681 of *Lecture Notes in Computer Science*, 65–72 (Springer, 2014).

23. Markovic, D. & Gros, C. Self-organized chaos through polyhomeostatic optimization. *Physical Review Letters* **105**, 068702 (2010).

24. Marković, D. & Gros, C. Intrinsic adaptation in autonomous recurrent neural networks. *Neural Computation* **24**, 523–540 (2012).

25. Intrator, N. & Cooper, L. N. Objective function formulation of the bcm theory of visual cortical plasticity: Statistical connections, stability conditions. *Neural Networks* **5**, 3–17 (1992).

26. Triesch, J. A gradient rule for the plasticity of a neuron's intrinsic excitability. In *Artificial Neural Networks: Biological Inspirations–ICANN 2005*, 65–70 (Springer, 2005).

27. Friston, K. The free-energy principle: a unified brain theory? *Nature Reviews Neuroscience* **11**, 127–138 (2010).

28. Prokopenko, M. *Guided self-organization: Inception*, vol. 9 (Springer, 2013).

29. Linkerhand, M. & Gros, C. Generating functionals for autonomous latching dynamics in attractor relict networks. *Scientific Reports* **3**, 2042 (2013).

30. Gros, C. Generating functionals for guided self-organization. In Prokopenko, M. (ed.) *Guided Self-Organization: Inception*, 53–66 (Springer, 2014).

31. Sitt, J. D., Amador, a., Goller, F. & Mindlin, G. B. Dynamical origin of spectrally rich vocalizations in birdsong. *Physical Review E* **78**, 011905 (2008).

32. Dahlem, M. A. Migraine generator network and spreading depression dynamics as neuromodulation targets in episodic migraine. *Chaos* **23**, 046101 (2013).

33. Ernesti, J., Righetti, L., Do, M., Asfour, T. & Schaal, S. Encoding of periodic and their transient motions by a single dynamic movement primitive. In *Humanoid Robots (Humanoids), 2012 12th IEEE-RAS International Conference on*, 57–64 (2012).

Acknowledgements

The work of B.S. was supported by the European Union and the State of Hungary, co-financed by the European Social Fund in the framework of TÁMOP 4.2.4.A/2-11-1-2012-0001 National Excellence Program.